REPORT

BATTERIES

Highly elastic binders integrating polyrotaxanes for silicon microparticle anodes in lithium ion batteries

Sunghun Choi,* Tae-woo Kwon,* Ali Coskun,† Jang Wook Choi†

Lithium-ion batteries with ever-increasing energy densities are needed for batteries for advanced devices and all-electric vehicles. Silicon has been highlighted as a promising anode material because of its superior specific capacity. During repeated charge-discharge cycles, silicon undergoes huge volume changes. This limits cycle life via particle pulverization and an unstable electrode-electrolyte interface, especially when the particle sizes are in the micrometer range. We show that the incorporation of 5 weight % polyrotaxane to conventional polyacrylic acid binder imparts extraordinary elasticity to the polymer network originating from the ring sliding motion of polyrotaxane. This binder combination keeps even pulverized silicon particles coalesced without disintegration, enabling stable cycle life for silicon microparticle anodes at commercial-level areal capacities.

The use of silicon (Si) for anodes has received much attention from the battery community because of its high specific capacity (over 3000 mAh g^{-1}) as part of the development of lithium (Li)–ion battery applications requiring high energy densities, such as all-electric vehicles (*1*–*3*). Although the massive volume change of Si during repeated charge-discharge cycles has been identified as the main origin of insufficient cycle lives of Si anodes, it has recently been recognized that binders can contribute substantially to improving their cycle lives (*4*, *5*).

Conventional polyvinylidene difluoride (PVDF) binders are not appropriate for Si anodes because of their weak van der Waals interactions with Si and the copper current collector (*4*–*14*). Some potential solutions include diverse covalent (*6*, *7*) and noncovalent (*8*–*12*) interactions in order to enhance the binding affinity between the binder and Si as well as between binders. Three-dimensional polymer networks have also been reported because linear polymers with poorly defined interchain interactions are not able to endure the structural instability of the Si electrode during cycling (*13*, *14*).

Although these binders improved the cycle lives of Si nanoparticle anodes, achieving long-term cycle life remains challenging for Si microparticle (SiMP) anodes with commercial levels of electrode loadings (*9*, *15*). SiMPs are more susceptible to pulverization during the volume expansion of Si as compared with their nanoparticle counterparts, which renders even recently reported high-performance polymer binders ineffective. It is generally accepted that the binder is not solely capable of resolving the issues related with practical SiMP anodes (*9*).

Having noticed that stress dissipation during the volume expansion of Si is key to the robust operation of Si anodes, we considered whether the mode of action of a pulley would work as a plausible stress-release mechanism. A series of pulleys, in which some are fixed at one end and others are free to move along the thread, lower the force required to lift an object in proportion to the number of moving pulleys involved (Fig. 1A). We developed a binder for SiMP anodes in which a small amount [5 weight % (wt %) of the binder portion] of ring-slide polyrotaxane (PR)—comprising polyethylene glycol (PEG) threads and α-cyclodextrin (α-CD) rings functionalized with 2-hydroxypropyl moieties—are covalently integrated with a conventional linear binder, polyacrylic acid (PAA) (Fig. 1B). Even though some of the polyrotaxane's ring components are covalently bonded to the PAA chains, they can still move freely along the thread component, thus serving like moving pulleys to substantially lower the tension exerted on the polymer network. The incorporation of only 5 wt % polyrotaxane into PAA renders the resulting polymer network highly stretchable and elastic, which makes even pulverized Si particles remain coalesced without disintegration during repeated (de)lithiation. Polyrotaxanes have also been recently adopted (*16*, *17*) for the demonstration of extremely elastic hydrogels.

The polyrotaxane was synthesized by the threading-followed-by-stoppering approach (figs. S1 to S4; details of the synthetic procedures are given in the supplementary materials, materials and methods) (*18*, *19*). α-CDs were threaded to the amine-functionalized PEG thread (molecular weight = ~20,000), which was subsequently stoppered with 1-fluoro-2,4-dinitrobenzene upon mechanical mixing in *N*,*N*-dimethylformamide (DMF) at room temperature. The –OH groups of α-CDs were further functionalized with propylene oxide to incorporate 2-hydroxypropyl moieties. The dual component binder PR–PAA was obtained by cross-linking some of the ring components of polyrotaxane with the PAA through ester bond formation (Fig. 1B and fig. S5). In their pristine state, the functionalized α-CD rings are expected to be distributed randomly along the PEG thread. However, once the SiMPs are expanded during lithiation, the stretching of polyrotaxane and PAA chains leads to the movement of the ring components closer to each other to reduce mechanical stress. Upon subsequent delithiation, the rings return from this high-energy state to their pristine state via entropic repulsion (*20*). As the SiMPs are pulverized during battery cycling (*21*, *22*), the ring sliding of polyrotaxanes keeps the pulverized Si particles coalesced, which is critical for preserving the electrode morphology. In contrast, a simple linear PAA binder without polyrotaxanes cannot perform such functions; thus, pulverized Si particles remain apart, and patchy solid electrolyte interphase (SEI) layers grow in the interparticle space (Fig. 1C). After prolonged cycling, SEI layers tend to grow continuously, leading to electrical disconnection between Si particles. Most of the previous binder approaches rely on the covalent or noncovalent cross-linking between polymer chains that eventually fail to sustain electrode integrity during repeated volume change of Si.

The impact of the polyrotaxane cross-linking was revealed by examining the mechanical properties of a PR-PAA film (supplementary materials, materials and methods). In general, the stretching behavior of a polymer film can be classified into three categories (Fig. 2A): nonlinear softening (r shape), linear elastic (Hookean), and nonlinear stiffening (J shape). Nonlinear stiffening behavior is often found in biological systems, such as spider silks and arterial walls, in which high elasticity is critical for preserving the main body or organ framework in response to external force (*23*–*25*). By contrast, nonlinear softening tends to undergo plastic deformation after a critical strain and thus may not recover the original network structure during repeated stretching cycles. Another noticeable feature with the nonlinear stiffening behavior is smaller stress accumulation with respect to an increase in strain, as can be expected from its J-shaped curve. This property equally implies that the fracture of the given network does not take place until a higher strain as compared with those of the other two types. Even after the fracture occurs, nonlinear stiffening would be more resistant against crack propagation (*23*).

Graduate School of Energy, Environment, Water, and Sustainability (EEWS) and KAIST Institute (KI) NanoCentury, Korea Advanced Institute of Science and Technology (KAIST), Daejeon 34141, Republic of Korea.
*These authors contributed equally to this work.
†Corresponding author. Email: coskun@kaist.ac.kr (A.C.); jangwookchoi@kaist.ac.kr (J.W.C.)

As displayed in Fig. 2B, the PAA film exhibited an r-shaped curve in its stress-strain plot, and most of the existing polymer binders are expected to follow the same trend. The PAA film ruptures at a strain of ~37% regardless of the stretching direction. At this point, it is anticipated that interchain hydrogen bonds break apart. By contrast, the PR-PAA film showed a curve that can be divided into two regimes: r-shaped (point 1 to 2) and J-shaped (point 2 to 3). In the r-shaped regime, PAA chains are rearranged along the load direction, with some of the hydrogen bonds being simultaneously cleaved. In this regime, the ring sliding of polyrotaxanes also reduces the stress to some degree, making the modulus lower than that of the PAA film. Upon entry into the J-shaped regime with further increase in strain, the ring sliding of polyrotaxanes plays a more dominant role in releasing the stress, allowing the PR-PAA film not to rupture until 390% strain. The entropic repulsion between agglomerated α-CD rings endows the polymer film with sufficient resilience to follow the same trajectory in the opposite direction of strain. When the stretch-recovery cycles were repeated in the sequence of 100, 150, and 200% strain limits, the PR-PAA film showed robust behavior (Fig. 2C). Even for the same strain limits, the curve shape became closer to a J shape with repeated stretch-recovery cycles because of the rearrangement of the PAA network that relies less on interchain hydrogen bonds. As expected, this trend is more pronounced in the initial several cycles with 100% strain.

The effect of the binder on the electrochemical performance of SiMP anodes was examined with half-cell measurements by using Li metal as counter/reference electrode (details of the cell preparation and electrochemical measurements are given in the supplementary materials, materials and methods). Each electrode is composed of SiMPs (diameter, 2.1 μm on average) (fig. S6), binder, and super P (Timcal, Switzerland) in a weight ratio of 8:1:1. At a fixed areal capacity of 3.18 mAh cm^{-2}, the electrode based on PR-PAA (denoted as PR-PAA-SiMP) showed a higher reversible capacity of 2971 mAh g^{-1} in the precycling at 0.03 3C (100 mA g^{-1}) compared with that of the PAA-SiMP electrode (2579 mAh g^{-1}) (Fig. 3A). The lessened particle disintegration of the PR-PAA–SiMP electrode largely mitigates electrolyte decomposition and thus produces a smaller amount of SEI layer (fig. S7, cross-sectional images), leading to an initial Coulombic efficiency of 91.22%, which is higher than that of the PAA-SiMP electrode (81.61%) and is even as high as those of typical graphite electrodes (*26*, *27*).

The PR-PAA–SiMP electrode exhibited far better cycling performance as compared with that of the PAA-SiMP electrode. When measured at 0.2 C (0.64 mA cm^{-2}), the PR-PAA–SiMP with an initial areal capacity of 2.67 mAh cm^{-2} preserved 2.43 mAh cm^{-2} after 150 cycles (Fig. 3B), corresponding to 91% capacity retention. By contrast, when measured under the same condition the PAA-SiMP electrode began to lose its capacity from the outset and retained only 48% of the initial capacity after 50 cycles. The Coulombic efficiency of the PR-PAA–SiMP increased to 97.37% at the first cycle upon C-rate change (0.033 to 0.2 C) and then rose to 99.10 and 99.82% at the fourth and 22nd cycle, respectively (Fig. 3B, inset). The average Coulombic efficiency in cycles 23 to 150 was 99.64%. In a separate measurement (Fig. 3C) of the PR-PAA–SiMP with 2.68 mAh cm^{-2} at 0.2 C (1 C = 3.12 mA cm^{-2}), once the cell had become stabilized for 10 cycles upon C-rate increase from 0.2 to 0.4 C, 85% of the capacity was retained for the remaining 370 cycles. For this measurement, the Li metal counter electrode had to be switched with a fresh one at the 220th cycle (arrow mark) to ensure that the degradation of the Li metal counter electrode (fig. S8) at a relatively high areal current density of 1.25 mA cm^{-2} did not affect the cyclability of the PR-PAA–SiMP. In fact, the capacity of the same PR-PAA–SiMP without switching the Li metal counter electrode decayed seriously at around the 250th cycle (red curve). The cycling data measured at different C-rates is presented in fig. S9. When examined for Si nanoparticles (diameter, ~50 nm), PR-PAA showed better cyclability than that of PAA (fig. S10). However, the effect of the binder was not as pronounced as that for SiMPs, thus indicating the different nature of Si nanoparticles and SiMPs in terms of binder design. In addition, a separate test with a film of PR-PAA alone verifies its electrochemical stability in the given anode potential range (fig. S11).

The high reversibility of the PR-PAA–SiMP prompted us to carry out a full-cell test in pairing with $LiNi_{0.8}Co_{0.15}Al_{0.05}O_2$ (NCA) cathode with a specific capacity of 188.7 mAh g_{NCA}^{-1} at 0.03 C (fig. S12). The negative/positive (*n*/*p*) ratio of the full-cell was set to 1.15. When tested at 0.03 C (1 C = 190 mA g_{NCA}^{-1}), the full-cell exhibited an areal

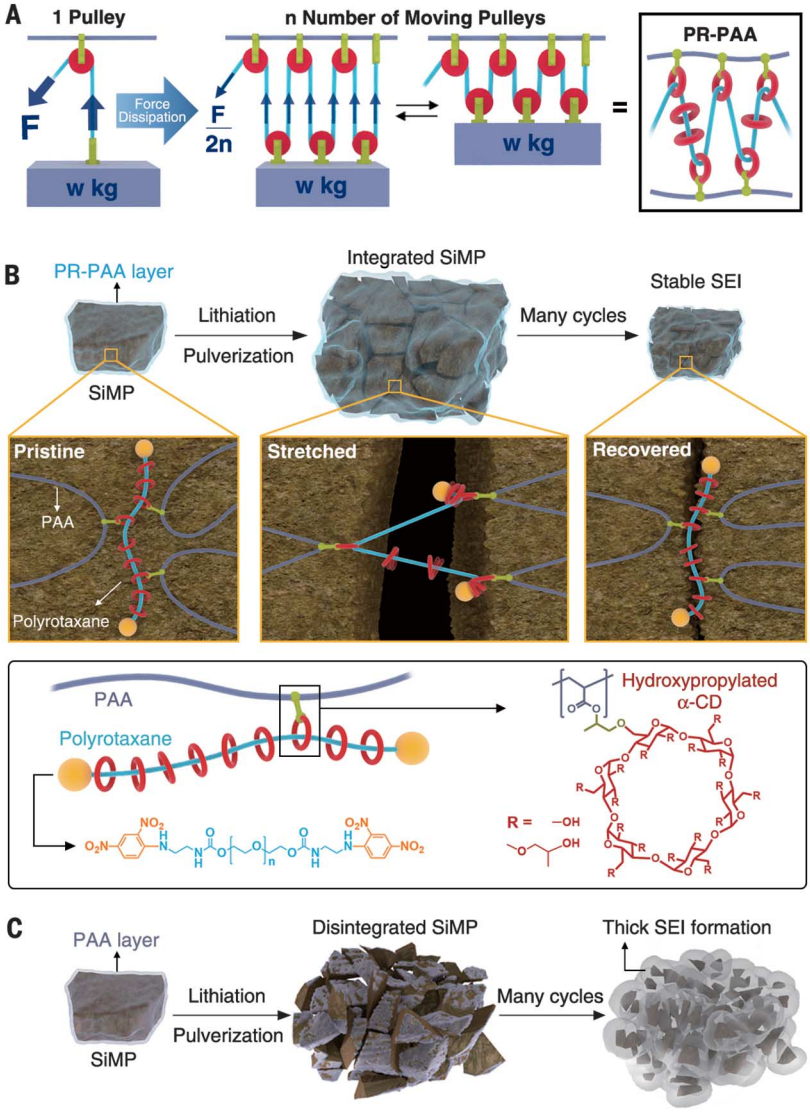

Fig. 1. Proposed stress dissipation mechanism of PR-PAA binder for SiMP anodes. (**A**) The pulley principle to lower the force in lifting an object. (**B**) Graphical representation of the operation of PR-PAA binder to dissipate the stress during repeated volume changes of SiMPs, together with chemical structures of polyrotaxane and PAA. (**C**) Schematic illustration of the pulverization of the PAA-SiMP electrode during cycling and its consequent SEI layer growth.

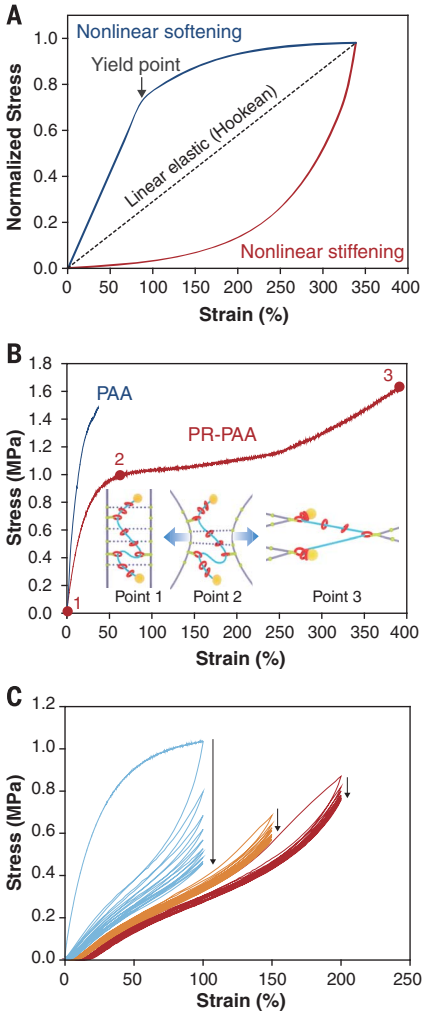

Fig. 2. Mechanical properties of PR-PAA and PAA. (**A**) Stress-strain behaviors of three representative modes. (**B**) Comparison of stress-strain curves of PR-PAA and PAA films and the proposed network configurations of PR-PAA at three strain points. (**C**) Stress-strain curves of PR-PAA for 10 stretch-recovery cycles with different strain limits.

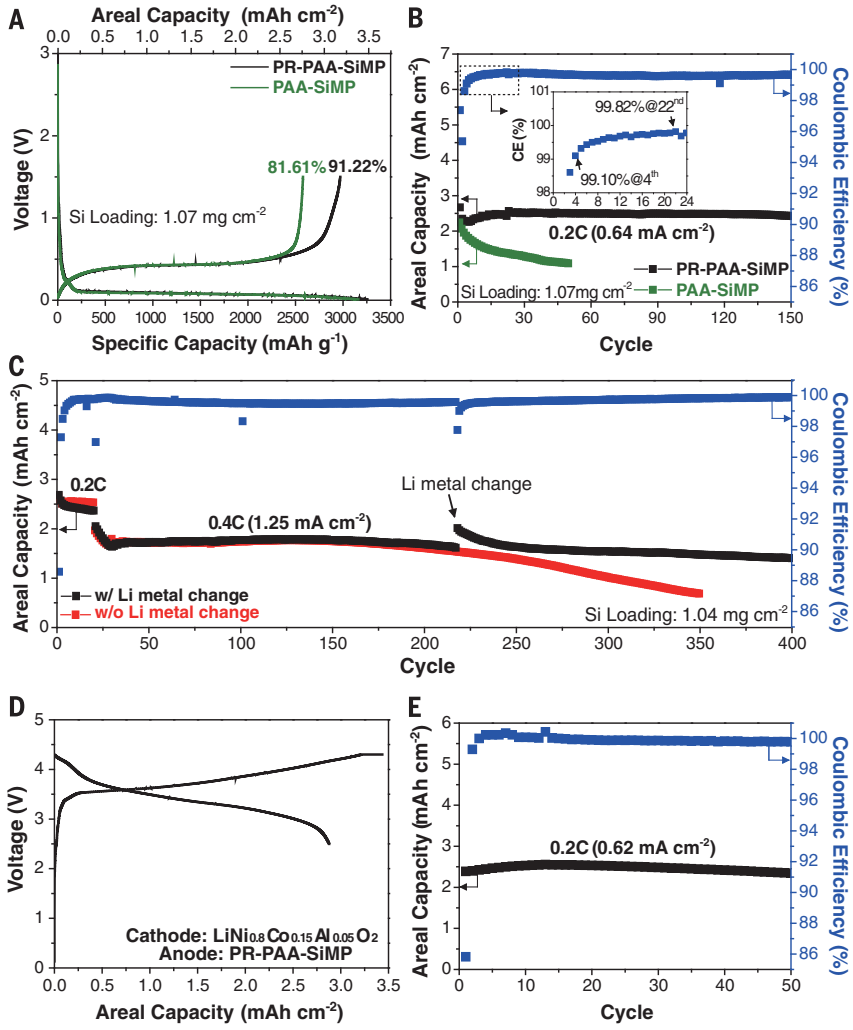

Fig. 3. Electrochemical performances of SiMP electrodes incorporating PR-PAA and PAA as binders. (**A**) The initial charge-discharge profiles of the PR-PAA–SiMP and PAA-SiMP electrodes when measured at 0.033 C (100 mA g^{-1}). (**B**) Discharging capacity retentions of both electrodes when measured at 0.2 C (600 mA g^{-1}), along with the Coulombic efficiencies of the PR-PAA–SiMP electrode. (Inset) Magnified view of the Coulombic efficiencies in the first 24 cycles. Si loading, 1.07 mg cm^{-2}. (**C**) Discharging capacity retention and Coulombic efficiencies of the PR-PAA–SiMP electrode when cycled at 0.2 and 0.4 C. 1 C = 3.12 mA cm^{-2}. Si loading, 1.04 mg cm^{-2}. The black arrow indicates the point when the Li metal counter electrode is replaced with a fresh one. (**D**) The initial charge-discharge profile of the SiMP–$LiNi_{0.8}Co_{0.15}Al_{0.05}O_2$ full cell at 0.03 C (1 C = 190 mA g_{NCA}^{-1}) and (**E**) its cycling performance at 0.2 C, along with the Coulombic efficiencies. The *n/p* ratio based on the capacities of both electrodes is 1.15.

capacity of 2.88 mAh cm^{-2} (Fig. 3D). The areal capacities covered in Fig. 3 fall in the range of those of current commercial Li-ion batteries. Furthermore, the full-cell showed decent cyclability, such as 98% retention of the original capacity after 50 cycles (Fig. 3E) and an average Coulombic efficiency of 99.92% in the cycle numbers of 2 to 50, confirming the sustainable operation of the PR-PAA–SiMP in a practical cell setting.

The critical role of PR-PAA on the electrochemical performance was unveiled through the analysis of electrode morphology imaged with scanning electron microscopy (SEM). At pristine states, the cross sections of the PR-PAA–SiMP and PAA-SiMP electrodes showed similar thickness (9.8 μm) and particle size distributions (Fig. 4, A and B). However, both electrodes exhibited a drastic difference in those properties after the 10th delithiation (fig. S13, electrochemical results); the thickness of the PR-PAA–SiMP and PAA-SiMP electrodes increased to 12.1 and 22.8 μm, respectively (Fig. 4, C and D), reflecting the enhanced stability of the SEI layer of the PR-PAA–SiMP. A compositional analysis of the SEI layer also showed distinct features between both electrodes, as described in fig. S14.

The top-viewed images of both electrodes portray consistent results. Whereas the PR-PAA–SiMP electrode kept even pulverized Si particles coalesced (Fig. 4E), the PAA-SiMP electrode (Fig. 4F) suffers from uncontrolled growth of SEI layers among pulverized particles. This SEI layer growth explains the much larger increase in thickness of the PAA-SiMP electrode (Fig. 4D). A large areal analysis verifies that the coalescence of pulverized particles is valid throughout the PR-PAA–SiMP electrode (figs. S15 to S17; details of the large area analysis are given in the supplementary materials, materials and methods). All images in Fig. 4 were obtained in back-scattered electron mode because back-scattered electrons can capture the objects in deeper regions (up to 400 to ~500 nm) than secondary electron mode with limited analysis depth (<50 nm), with enhanced brightness for objects with high atomic numbers (*28*). Thus, in our electrodes, Si particles can be visualized more clearly without disturbance of the SEI layer compared with the secondary

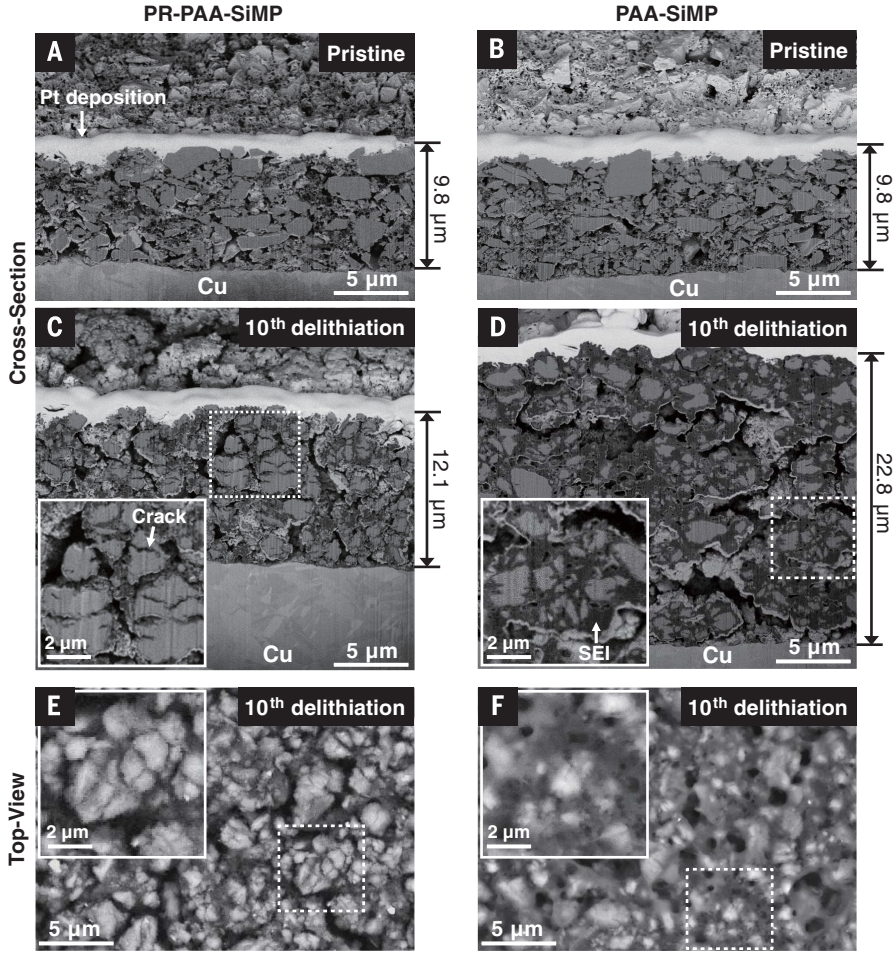

Fig. 4. Ex situ SEM characterization of SiMP electrodes based on PR-PAA and PAA binders before and after cycling. (**A** and **B**) Cross-sectional images of the (A) PR-PAA–SiMP and (B) PAA-SiMP electrodes before cycling. (**C** and **D**) Cross-sectional images of the (C) PR-PAA–SiMP and (D) PAA-SiMP electrodes after the 10th delithiation. Si loading, 0.70 mg cm^{-2}; C-rate, 0.2 C. The insets in (C) and (D) are magnified images from the white dotted boxes. (**E** and **F**) Top-viewed SEM images of the (E) PR-PAA–SiMP and (F) PAA-SiMP electrodes after the 10th delithiation. All images in this figure were obtained under back-scattered electron mode. The thickness of electrodes was adjusted because all cross sections were imaged at a 52° tilt angle.

electron mode (fig. S18). The superior role of PR-PAA binder was also revealed by more robust adhesion of the electrode film onto the current collector during cycling (fig. S19).

The incorporation of sliding-ring polyrotaxane alters the mechanical properties of traditional binders such as PAA and leads to a highly elastic binder network engaging the sliding motion of polyrotaxane. This can resolve the issues originating from the volume expansion of Si anodes, even with commercially viable electrode conditions and micrometer-scale particle dimensions. The introduction of a mechanical bond in the form of a polyrotaxane keeps pulverized particles together without disintegration and therefore offers a general strategy to extend the cycle lives of high-capacity Li-ion battery electrodes that undergo large volume changes during cycling. These approaches may help increase the Si content in graphite-dominant electrodes and thus the energy densities of Li-ion batteries.

REFERENCES AND NOTES

1. B. Dunn, H. Kamath, J.-M. Tarascon, *Science* **334**, 928–935 (2011).
2. J. W. Choi, D. Aurbach, *Nat. Rev. Mater.* **1**, 16013 (2016).
3. M. N. Obrovac, L. Christensen, D. B. Le, J. R. Dahn, *J. Electrochem. Soc.* **154**, A849–A855 (2007).
4. I. Kovalenko *et al.*, *Science* **334**, 75–79 (2011).
5. J. Li, R. B. Lewis, J. R. Dahn, *Electrochem. Solid-State Lett.* **10**, A17–A20 (2007).
6. B. Koo *et al.*, *Angew. Chem. Int. Ed.* **51**, 8762–8767 (2012).
7. Z.-J. Han, N. Yabuuchi, S. Hashimoto, T. Sasaki, S. Komaba, *ECS Electrochem. Lett.* **2**, A17–A20 (2013).
8. T. W. Kwon *et al.*, *Adv. Mater.* **26**, 7979–7985 (2014).
9. C. Wang *et al.*, *Nat. Chem.* **5**, 1042–1048 (2013).
10. H. Zhao *et al.*, *Nano Lett.* **15**, 7927–7932 (2015).
11. T. W. Kwon *et al.*, *ACS Nano* **9**, 11317–11324 (2015).
12. N. Salem, M. Lavrisa, Y. Abu-Lebdeh, *Energy Technol.* **4**, 331–340 (2016).
13. M. Murase *et al.*, *ChemSusChem* **5**, 2307–2311 (2012).
14. Y. K. Jeong *et al.*, *Energy Environ. Sci.* **8**, 1224–1230 (2015).
15. Y. Li *et al.*, *Nat. Energy* **1**, 15029 (2016).
16. A. Bin Imran *et al.*, *Nat. Commun.* **5**, 5124 (2014).
17. Y. Okumura, K. Ito, *Adv. Mater.* **13**, 485–487 (2001).
18. A. Harada, J. Li, M. Kamachi, *Nature* **356**, 325–327 (1992).
19. F. M. Raymo, J. F. Stoddart, *Chem. Rev.* **99**, 1643–1664 (1999).
20. K. Ito, *Polym. J.* **44**, 38–41 (2012).
21. X. H. Liu *et al.*, *ACS Nano* **6**, 1522–1531 (2012).
22. U. Kasavajjula, C. Wang, A. J. Appleby, *J. Power Sources* **163**, 1003–1039 (2007).
23. S. W. Cranford, A. Tarakanova, N. M. Pugno, M. J. Buehler, *Nature* **482**, 72–76 (2012).
24. J. E. Gordon, *Structures* (Penguin Books, London, 1978).
25. G. A. Holzapfel, T. C. Gasser, R. W. Ogden, *J. Elast.* **61**, 1–48 (2000).
26. M. Yoshio, H. Wang, K. Fukuda, Y. Hara, Y. Adachi, *J. Electrochem. Soc.* **147**, 1245–1250 (2000).
27. W. Guoping *et al.*, *Solid State Ion.* **176**, 905–909 (2005).
28. J. I. Goldstein *et al.*, *Scanning Electron Microscopy and X-Ray Microanalysis* (Plenum Press, 1981).

ACKNOWLEDGMENTS

We acknowledge the support from the National Research Foundation of Korea (NRF) grant funded by the Korean government (MEST) (NRF-2015R1A2A1A05001737). S.C., T.-w.K., A.C., and J.W.C. are inventors on a Korean patent application (no. 10-2016-0181036) submitted by the Korea Advanced Institute of Science and Technology that covers binder designs.

SUPPLEMENTARY MATERIALS

www.sciencemag.org/content/357/6348/279/suppl/DC1
Materials and Methods
Figs. S1 to S19
References (*29*–*34*)

18 November 2016; resubmitted 3 March 2017
Accepted 30 May 2017
10.1126/science.aal4373

Science

Highly elastic binders integrating polyrotaxanes for silicon microparticle anodes in lithium ion batteries

Sunghun Choi, Tae-woo Kwon, Ali Coskun and Jang Wook Choi

Science **357** (6348), 279-283.
DOI: 10.1126/science.aal4373

A stretchy binder protects the silicon

A challenge in using silicon particles for lithium batteries is that the large volume changes during charge-discharge cycling cause the particles to fracture, which builds up an insulating interface layer. Choi *et al.* show that traditional binder materials used to cushion the silicon particles can be improved by adding small amounts of polyrotaxanes (see the Perspective by Ryu and Park). The molecules consist of multiple rings that are strung along a linear segment and stoppered at each end. Some of the rings are anchored to the polymer binder, whereas others float freely, yielding a highly mobile but connected network that anchors the binder, and thus the silicon particles, together.

Science, this issue p. 279; see also p. 250